Variation after parity projection calculation with the Skyrme interaction for light nuclei

H. Ohta and K. Yabana

Institute of Physics, University of Tsukuba, Tsukuba 305-8571, Japan

T. Nakatsukasa*

Department of Physics, Tohoku University, Sendai 980-8578, Japan

A self-consistent calculation with variation after parity projection is proposed to study both ground and excited states of light nuclei. This procedure provides description of the ground state incorporating some correlation effects, and self-consistent solutions for the excited states of negative parity. For flexible description of nuclear shapes, single particle orbitals are represented on a uniform grid in the three-dimensional Cartesian coordinates. The angular momentum projection is performed after variation to calculate rotational spectra. To demonstrate the usefulness of the method, results are shown for two $N=Z$ nuclei, ^{20}Ne and ^{12}C, for which clustering correlations are known to be important. In the ^{20}Ne nucleus, both cluster-like and shell-model-like states are described simultaneously in the present framework. For ^{12}C nucleus, the appearance of three-alpha clustering correlation in the ground state is investigated in relation to the strength of the two-body spin-orbit interaction.

Nuclear mean-field calculations have been successful for systematic description of nuclear ground state properties with a few adjustable parameters [1]. The mean-field theory has also been extensively applied to description of excited states. For example, collective vibrational as well as single particle-hole excitations are described by the random phase approximation which is equivalent to a small amplitude limit of the time-dependent mean-field dynamics. Excited states may also be described as local-minimum solutions if there is more than one self-consistent solution in the static calculation. In principle, the generator coordinate method is expected to provide a unified description for any kind of excitations. However, in practice, one need to specify a few important generator coordinates in advance by physical intuition.

In this article, we present an attempt to describe both ground and excited states in the self-consistent approach with the variation after parity projection (VAPP). For an even-even nucleus, the lowest energy positive-parity solution describes the ground state in which the correlation beyond the mean field is incorporated to a certain extent. Self-consistent negative-parity solutions should correspond to the negative-parity excited states.

The theory of the variation after projection (VAP) of the symmetry-violating internal state has a long history [2]. However, practical applications with full variation of single-particle orbitals are rather few even for projection with respect to the parity. Previously we achieved the VAPP calculation employing the uniform grid representation in the three-dimensional (3D) Cartesian coordinates in which simple BKN interaction was used [3]. In the ordinary mean-field calculations, one usually obtains self-consistent solu-

tions with axial and reflection symmetries for most nuclei. However, in the VAPP calculations, the self-consistent solutions are found to violate these symmetries. A preliminary report on the realistic calculations employing the Skyrme interaction has been presented in Refs. [4,5].

We apply the method to light $N=Z$ nuclei, ^{20}Ne and ^{12}C. There are several reasons why we consider the light nuclei. For light nuclei, the VAP may significantly modify the mean-field solutions and lead to the energy gain by the projection. In the excited states of light nuclei, various cluster structures have been found to appear. They have been successfully analyzed with the microscopic cluster models in which the VAP calculation was carried out [6]. The present approach is useful to understand the mechanism for the appearance of the cluster structures. Finally, there are rapid progresses in the experimental research on light unstable nuclei. The present framework will be useful to analyze and predict structures of unstable nuclei.

The antisymmetrized molecular dynamics (AMD) method developed by Kanada-En'yo and Horiuchi [7] has been utilized to describe clustering phenomena in light stable and unstable nuclei. In the simplest version of AMD, the method is identical to the VAPP with a restricted Slater determinant in which each orbital is a Gaussian wave packet. This may be regarded as an approximation to our present approach. The feasibility of the AMD allows them to perform the variation after angular momentum projection [8]. On the other hand, the present work brings more accurate description of the single particle orbitals, and establishes an intimate link to the Skyrme Hartree-Fock theory.

We start with a brief description of the theory [3]. We consider an arbitrary Slater determinant $\Phi = (1/\sqrt{N!})\det\{\phi_i(x_j)\}$, with $x=(\vec{r}, \sigma)$, the space and spin coordinates. We apply the parity projection operator for this Slater determinant, $\Phi^{(\pm)} = (1/\sqrt{2})(1 \pm \hat{P})\Phi$, where $\hat{P}$ is the space inversion operator. We then consider the energy expec-

————
*Present address: Institute of Physics, University of Tsukuba, Tsukuba 305-8571, Japan.

tation value for the states with definite parity, $\Phi^{(\pm)}$, and make a variation with respect to the single particle orbitals ϕ_i,

$$\frac{\delta}{\delta\phi_i^*}\left[\frac{\langle\Phi^{(\pm)}|\hat{H}|\Phi^{(\pm)}\rangle}{\langle\Phi^{(\pm)}|\Phi^{(\pm)}\rangle} - \sum_{i,j}\epsilon_{ij}\langle\phi_i|\phi_j\rangle - \vec{\eta}\sum_i\langle\phi_i|\vec{r}|\phi_i\rangle\right] = 0 \tag{1}$$

Here we imposed two kinds of constraints in the above variation [3]. The first one with the Lagrange multipliers ϵ_{ij} is introduced to orthonormalize single particle orbitals, ϕ_i. The second with the multiplier $\vec{\eta}$ is to coincide the center-of-mass of the wave function Φ with the origin of the coordinate, $\Sigma_i\langle\phi_i|\vec{r}|\phi_i\rangle = 0$. This constraint assures that the parity operation is made with respect to the center-of-mass of the nucleus and minimizes the occurrence of the spurious center-of-mass excitations by the parity projection.

The variation of Eq. (1) yields the following self-consistent equation:

$$(h - \vec{\eta}\cdot\vec{r})\phi_i \pm \langle\Phi|\hat{P}|\Phi\rangle\left\{h_P\tilde{\phi}_i - \sum_j\tilde{\phi}_j\langle\phi_j|h_P|\tilde{\phi}_i\rangle\right\}$$
$$+ (E^{(\pm)} - E)\tilde{\phi}_i = \sum_j\epsilon_{ij}\phi_j \tag{2}$$

where h is the usual Hartree-Fock Hamiltonian. h_P has the same structure as h, however, all the densities are replaced with the transition densities which are the matrix elements of density operators between the wave function Φ and its parity-inverted state $\hat{P}\Phi$. $E^{(\pm)}$ is the energy expectation value with respect to the wave function $\Phi^{(\pm)}$, while E is with respect to Φ. $\tilde{\phi}_i$ is defined by

$$\tilde{\phi}_i = \sum_j\hat{P}\phi_j(B^{-1})_{ji} \tag{3}$$

with $B_{ij} = \langle\phi_i|\hat{P}|\phi_j\rangle$.

In the practical calculations, Eq. (2) is not solved directly. Instead, the imaginary-time method is employed in which the left-hand-side of Eq. (2) is used as the gradient of the energy functional. We discretize the 3D Cartesian coordinates into uniform square grid and represent the single particle wave functions on the grid points. The grid spacing is taken to be 0.8 fm, and the grid points inside a sphere of radius 7.2 fm are used in the calculations below.

After obtaining the self-consistent solutions, we make the angular momentum projection (AMP) to calculate rotational spectra. The self-consistent solutions in the VAPP are usually not axially symmetric. Therefore, one must perform three-dimensional rotation in Euler angles, $\Omega = (\alpha, \beta, \gamma)$, for the AMP. We define the AMP state as usual,

$$|\Phi_{MK}^{J(\pm)}\rangle = \frac{2J+1}{8\pi^2}\int d\Omega D_{MK}^{J*}(\Omega)R(\Omega)|\Phi^{(\pm)}\rangle, \tag{4}$$

where $R(\Omega)$ is the rotation operator and $D_{MK}^J(\Omega)$ is the Wigner's D-function. We then define relevant matrix elements, $h_{KK'}^{J(\pm)}$ and $n_{KK'}^{J(\pm)}$. The Hamiltonian matrix element $h_{KK'}^{J(\pm)}$ is given by

$$h_{KK'}^{J(\pm)} = \langle\Phi_{MK}^{J(\pm)}|\hat{H}|\Phi_{MK'}^{J(\pm)}\rangle = \frac{2J+1}{8\pi^2}\int d\Omega D_{KK'}^{J*}(\Omega)$$
$$\times\langle\Phi|e^{-i\alpha\hat{J}_z}\hat{H}(1\pm\hat{P})e^{-i\beta\hat{J}_y}e^{-i\gamma\hat{J}_z}|\Phi\rangle, \tag{5}$$

and the similar expression for the norm matrix element, $n_{KK'}^{J(\pm)}$. For practice, we achieved the rotation of the single particle orbitals by successive rotations of a small angle. Following the Taylor expansion method for time evolution which was employed in the time-dependent Hartree-Fock calculations [9], we calculate the rotation of small angle $\Delta\alpha$ around z-axis by

$$\phi_i^{\alpha+\Delta\alpha} = \sum_{k=0}^{N_{max}}\frac{(\Delta\alpha)^k}{k!}(j_z)^k\phi_i^\alpha, \tag{6}$$

where N_{max} is taken to be 4. Typically, each Euler angle is discretized into 200 steps for α and γ, and into 400 steps for β. In Eq. (5), the integrations over Euler angles are achieved with discretization of 20 points for α and γ and 400 (all) points for β. It is important to divide rotations of three Euler angles into two and one; the rotations of the angles β and γ for the ket state, and the rotation of the angle α for the bra state, to reduce the computational costs.

We employ the Skyrme interaction in constructing the energy functional in Eq. (1). There is ambiguity in the choice of the density of density dependent force for off-diagonal matrix elements [10], which appear in Eqs. (1), (2), and (5). In this paper, we simply use corresponding transition densities for them. We will hereafter abbreviate the present scheme as the parity-projected Skyrme Hartree-Fock (PPSHF) method.

Before showing our results, we mention some problematic aspects of the Skyrme interaction in the present framework which we have encountered in the practical calculations. Since the Skyrme interaction has been so constructed to be used for a single Slater determinant state, it is by no means evident whether it may provide a reasonable description in the VAPP calculations. Indeed, we have observed that, if we make a variation of single particle orbitals without any restriction, we obtain an unphysical solution in which the time-reversal symmetry is violated in the ground state. For example, the total binding energy of ^{20}Ne in the ordinary Skyrme Hartree-Fock (SHF) calculation with SGII force is about 170 MeV, while we obtain the binding energy of 230 MeV with the PPSHF. Since the parametrization of the Skyrme interaction relevant to the time-odd component has not been fully tested, we restrict our wave function to be time-reversal invariant. Namely, we force nucleons either to fully occupy or unoccupy a pair of orbitals which are mutually related to each other by the time-reversal operation in the Slater determinant. This restriction removes most part of the problems. However, in the positive parity solutions of some light nuclei, we still encounter a problem that the density of the self-consistent solution shows a small but unphysical oscillation, namely, the density shows staggering in the neighboring grids. This problem can be overcome if we further ignore a part of the Skyrme energy functionals including terms $\vec{\rho}, \vec{j}, \vec{T}$ [11,12]. For a single Slater determinant with time-reversal invariance, these time-odd densities, $\vec{\rho}, \vec{j}$,

TABLE I. Self-consistent solutions of ^{20}Ne are summarized. The third row ("Energy (MF)") shows the results of ordinary SHF and PPSHF ($K^\pi=0^+$, $K^\pi=2^-$, $K^\pi=0^-$) before AMP. Total energy is shown for the ground state (SHF and $K^\pi=0^+$), while the excitation energies with respect to the ground state are shown for the excited states ($K^\pi=2^-$ and $K^\pi=0^-$). The fourth raw ("Energy (MF +AMP)") indicates the results for the lowest angular momentum state after the AMP. The fifth raw ("E_{LS}") is the expectation value of the two-body spin-orbit interaction. The β_2, γ, β_{30}, and β_{32}, are the density deformation of the internal single Slater determinant.

	$K^\pi=0^+$	$K^\pi=2^-$	$K^\pi=0^-$	SHF
Energy (EXP)	−160.645	+4.97	+5.78	−160.645
Energy (MF)	−168.232	+5.47	+7.96	−167.943
Energy (MF+AMP)	−171.333	+4.91	+6.42	
E_{LS}	−8.517	−15.350	−5.443	−8.775
β_2	0535	0.589	0.694	0.728
γ	0.0	0.0	0.0	0.0
β_{30}	0.314	0.0	0.576	0.0
β_{32}	0.0	0.178	0.0	0.0

$\vec{T}$, vanishes identically. However, this is not the case for transition densities between Φ and $\hat{P}\Phi$.

The problems are related to the fact that the superposition of two Slater determinants by the parity projection may represent more varieties of correlation effects than the single Slater determinant may do. We leave it an interesting future problem to find appropriate Skyrme energy functional to be used in the PPSHF framework. In the following calculations, we will employ SGII parameter set [13]. This force has been successful in describing the response properties of nuclei, although the absolute binding energies are not reproduced accurately.

We first show the results of ^{20}Ne. In Table I, the calculated results are summarized. The definition of the deformation parameters is in Ref. [14]. Octupole deformation parameters β_{31} and β_{33} are negligible and not shown. The positive-parity solution corresponds to the ground state. In the SHF calculation, this has a prolate shape with reflection symmetries. On the other hand, the PPSHF calculation gives the solution with substantial β_{30} deformation. The energy in the PPSHF calculation gets lower by 0.3 MeV from the ordinary SHF calculation.

There are two solutions in the negative parity. The lowest energy solution has a small β_{32} deformation as well as the prolate deformation. The next solution has a large β_{30} deformation as well as β_2. In the angular momentum projection, we found that the former solution is characterized by $K^\pi=2^-$ and the latter solution by $K^\pi=0^-$.

Previously we reported the existence of two local minima in the negative parity [4]. After careful examination, we have found that the $K^\pi=0^-$ solution is not a local minimum solution but decays into the $K^\pi=2^-$ solution after very long imaginary-time iterations (typically 5×10^3 steps with $\Delta t=10^{-3}$ MeV^{-1}). Reflecting different K^π value of these two states, they are almost orthogonal to each other. To examine the physical reality of the $K^\pi=0^-$ solution, we have per-
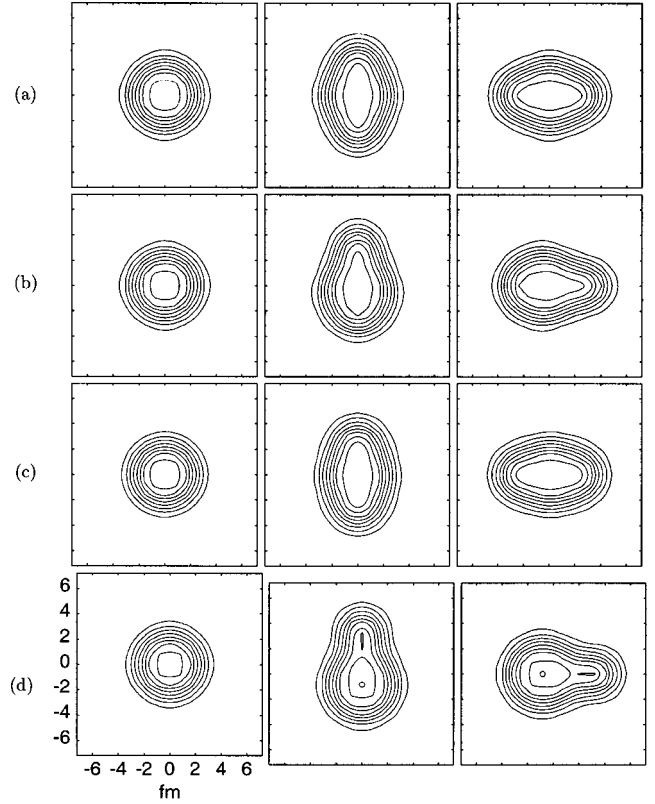

FIG. 1. Density distribution of the internal state in ^{20}Ne, in the xy, yz, and zx planes where x, y, and z axes represent the principal inertia axes, for (a) ground $K^\pi=0^+$ state of the SHF calculation, (b) ground $K^\pi=0^+$ state of PPSHF, (c) excited $K^\pi=2^-$ state of PPSHF, and (d) excited $K^\pi=0^-$ states of PPSHF, respectively. The side of each panel is 14.4 fm. The contour lines are plotted for every 0.02 fm^{-3}.

formed the imaginary-time evolution of this solution with an extra constraint that the wave function is orthogonal to the $K^\pi=2^-$ solution. In this procedure, we obtain a converged solution which is found to be almost the same as the original $K^\pi=0^-$ quasi-stable solution without the orthogonalization. Because of these observations and a good correspondence to the measured spectra as shown below, we consider that the $K^\pi=0^-$ solution is of physical significance.

Figure 1 shows density distribution of the internal Slater determinant Φ in the three planes which include two principal inertia axes. Figures 1(a) are the SHF calculation, and the Fig. 1(b) are the PPSHF for positive parity. They correspond to the ground state. Figures 1(c) and 1(d) are the PPSHF calculations for negative parity. Figures 1(c) is the lowest energy $K^\pi=2^-$ state, and Fig. 1(d) is the $K^\pi=0^-$. The nuclear shapes of Figs. 1(b) and 1(d) are characterized by the strong β_{30} deformation and are considered to reflect the α-^{16}O cluster structure. The clustering is stronger in the negative parity solution, which is consistent with the cluster model studies [6]. The lowest energy negative-parity solution shown in Fig. 1(c) looks prolate although it has a small β_{32} deformation.

As for the lowest negative parity state with $K^\pi=2^-$, the excitation energy before AMP (the energy difference between the negative- and positive-parity solutions) is 5.47 MeV and that after AMP (the energy difference between
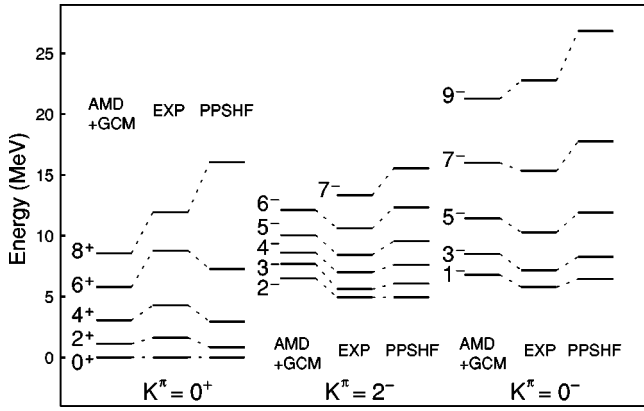
FIG. 2. Energy spectra of ^{20}Ne calculated with the AMP.

$J^{\pi}=0^{+}$ and $J^{\pi}=2^{-}$ solutions in the parity and angular momentum projections) is 4.91 MeV. These values are close to the measured 2^{-} excitation energy of ^{20}Ne, 4.97 MeV.

The next negative parity solution with $K^{\pi}=0^{-}$, which shows large β_{30} deformation, has α-^{16}O cluster structure, as mentioned before. The excitation energy before AMP is 7.96 MeV and that after AMP is 6.42 MeV, which are slightly higher than the measured excitation energy 5.78 MeV of the $J^{\pi}=1^{-}$ level. The different character of the two negative-parity solutions with $K^{\pi}=2^{-}$ and $K^{\pi}=0^{-}$ manifests clearly in the spin-orbit energy, E_{LS}, the expectation value of the two-body spin-orbit force. The $K^{\pi}=2^{-}$ solution has large spin-orbit energy which is supposed to reflect dominant shell-model-like $5p$-$1h$ configuration. The spin-orbit energy of $K^{\pi}=0^{-}$ solution is much smaller, even smaller than that in the ground state. This is consistent with the development of α-^{16}O cluster structure in the negative-parity states which was seen in the density distribution in Fig. 1.

In Fig. 2, we show the excitation spectra of ^{20}Ne after AMP. For three rotational bands of $K^{\pi}=0^{+}$, 2^{-}, and 0^{-}, calculated spectra are compared with measurements and with the results by the AMD (deformed AMD+GCM calculation with Gogny force) [15]. Since each band is well characterized by the K quantum number, we simply show the energies given by $E_{K}^{J(\pm)}=h_{KK}^{J(\pm)}/n_{KK}^{J(\pm)}$. Although the band head energies of 0^{+}, 2^{-}, and 1^{-} are described reasonably well, the calculated moment of inertia deviates from the measured value. The calculated moment of inertia is too large for the ground state band. On the other hand, the calculated moment of inertia for the negative parity bands is slightly too small, opposite to the positive parity band. The bandhead energy of the $K^{\pi}=2^{-}$ band in the AMD calculation is not as good as the PPSHF, probably because the present work has a better account of the single-particle wave functions.

The AMD method gives better description for the high spin levels, 6^{+}-8^{+} energy difference. In our calculation, the AMP is performed from a single intrinsic state, while a change of nuclear shape is shown as the angular momentum increases in the AMD calculation [15]. This indicates that, if we incorporate the cranking in the PPSHF framework, we might obtain better description for the higher angular momentum states. The discrepancy in the moment of inertia

TABLE II. Observed and calculated intra-band $B(E2)$ strengths of the $K^{\pi}=0^{+}$ and $K^{\pi}=2^{-}$ bands of ^{20}Ne. For the sake of comparison, we show results of the rotational model (Rot.) and the AMD+GCM [15]. The observed values are taken from Ref. [18]. The values enclosed by curly brackets in the rotational model (rot.) are adjusted to experimental ones.

$K^{\pi}=0^{+}$	$B(E2)_{obs}$	Rot.	AMD+GCM	PPSHF
$2^{+}\rightarrow 0^{+}$	57 ± 8	(57.0)	70.3	41.6
$4^{+}\rightarrow 2^{+}$	71 ± 7	81.4	83.7	59.9
$6^{+}\rightarrow 4^{+}$	66 ± 8	89.7	52.7	67.5
$8^{+}\rightarrow 6^{+}$	24 ± 8	93.9	21.0	75.1
$K^{\pi}=2^{-}$	$B(E2)_{obs}$	Rot.	AMD+GCM	PPSHF
$3^{-}\rightarrow 2^{-}$	113 ± 29	101	102.8	97.6
$4^{-}\rightarrow 3^{-}$	77 ± 16	75	77.8	73.5
$4^{-}\rightarrow 2^{-}$	34 ± 6	(34)	38.5	32.9
$5^{-}\rightarrow 4^{-}$	<808	53	84.5	52.6
$5^{-}\rightarrow 3^{-}$	84 ± 19	53	56.6	53.1
$6^{-}\rightarrow 5^{-}$	32 ± 13	39	29.9	39.7
$6^{-}\rightarrow 4^{-}$	55^{+23}_{-13}	66	64.0	67.0

looks similar between PPSHF and AMD calculations. At present, we do not have a definite answer for the origin of this discrepancy. The pairing correlation ignored in the present calculation may be a possible answer. Bender *et al.* calculated ground state bands of some light nuclei in the HFBCS+GCM+AMP scheme [16]. Their calculation slightly underestimates the moment of inertia, opposite to our result. In the mean-field calculations, it has also been pointed out that the moment of inertia is sensitive to the time-odd component which we ignored [17].

In Table II, we show observed and calculated intra-band $B(E2)$ strengths of the $K^{\pi}=0^{+}$ and $K^{\pi}=2^{-}$ bands of ^{20}Ne. For the sake of comparison, we show results of the rotational model (Rot.) and the AMD+GCM [15]. Our calculation well reproduces $B(E2)$ values of the 2^{-} band. For the 0^{+} band, our calculation somewhat underestimates the $B(E2)$ values of low angular momentum states. It should be noted that we do not introduce any effective charge. For $8^{+}\rightarrow 6^{+}$ transition, our result overestimates the $B(E2)$ value, and is close to the rotational model. This is because we made AMP calculations from a single configuration.

We next discuss ^{12}C. In the SHF calculations, one usually obtain spherical ground state for a ^{12}C nucleus, although the rotational spectra is observed experimentally. The spin-orbit interaction favors spherical structure to gain energy through $p_{3/2}$-$p_{1/2}$ splitting. If one weakens the spin-orbit interaction slightly, oblate deformation starts to appear in the ground state. We investigate change of the shape in the ground state by modifying the strength of the spin-orbit interaction, multiplying a constant factor x_{LS} to the two-body spin-orbit interaction of the Skyrme force. In Fig. 3, we show β_2 and β_{33} of the positive parity solution as a function of x_{LS}. The β_2 value in the ordinary SHF calculation is shown as well.

We have found that, in the PPSHF calculation, an oblate shape with substantial β_{33} deformation (triangle shape) ap-
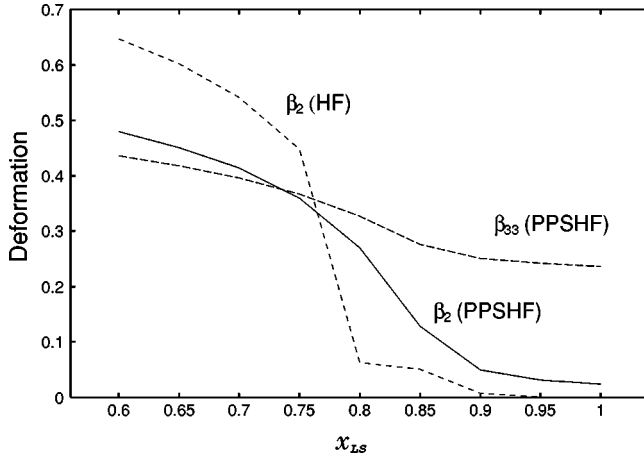
FIG. 3. Deformation of ^{12}C ground state as a function of x_{LS} which is a multiplicative factor for the two-body spin-orbit interaction.

pears if one employs a slightly weak spin-orbit interaction. This may be regarded as the appearance of the 3α clustering structure. The β_{33} deformation does not appear in the ordinary SHF calculation. In addition, the oblate deformation starts to appear at larger x_{LS} value in the PPSHF calculation than in the SHF. In the ordinary SHF calculation, the appearance of the oblate deformation starts abruptly at about $x_{LS} = 0.75 - 0.8$. Note that, in order to remedy the isotope-shift problem in Pb isotopes, the spin-orbit potential should be weakened by about 30 percent from the ordinary one [19].

We have examined AMP for solutions with different x_{LS} values, and have found that the ground state rotational band of $0^+, 2^+, 4^+$ is well described if we employ $x_{LS} = 0.8$. At this value of x_{LS}, we also made a calculation for negative parity solution. We show below the results with this strength of the spin-orbit interaction. The results are summarized for energies and deformations in Table III, for intrinsic density distribution in Fig. 4, and for the energy spectra in Fig. 5. Calculated $B(E2 : 2^+ \rightarrow 0^+)$ value is 5.14 e^2 fm^4 which should be compared with the observed value 7.8 ± 0.4 e^2 fm^4 [20].

As seen in Fig. 4(a), the nuclear shape is almost spherical in the ordinary SHF. At a slightly small x_{LS} value, oblate shape appears in the ordinary SHF calculation (Fig. 3). In spite of the strong β_2 and β_{33} deformation, the spin-orbit energy is still large in the PPSHF calculation, almost comparable to that in the spherical SHF calculation. This indicates that the closed $p_{3/2}$ configuration has still significant effects on the ground state.

The negative parity solution shows strong β_2 deformation with triaxiality. It has also strong octupole deformation, mainly β_{33} with small mixture of β_{31}. Reflecting this mixture in shape, two configurations with different K quantum numbers also coexist in the solution. Figure 4(c) shows that the 3α clustering is much more developed in the negative parity than in the ground state. The AMP calculation gives reasonable description for excitation energy. Because of γ deformation, not only 3^- and 4^- states but also 1^- and 2^- states appear as the side band.

It turns out that the structure of the negative parity solution in the PPSHF depends strongly on the x_{LS} value. If one

TABLE III. Calculated results of ^{12}C at $x_{LS} = 0.8$. The meaning of the listed quantities are the same as those in Table I.

	$K^\pi = 0^+$		SHF
		Negative parity	
Energy (EXP)	−92.162		−92.162
		+9.64	
Energy (MF)	−94.617		−94.492
		+11.15	
Energy (MF+AMP)	−96.499		
		+9.69	
E_{LS}	−13.229		−15.191
		−7.550	
β_2	0.271		0.069
		0.638	
γ	59.95°		60.00°
		27.77°	
β_{31}	0.0		0.0
		0.056	
β_{33}	0.327		0.0
		0.518	

employs the original Skyrme parametrization ($x_{LS} = 1.0$), we obtain $K^\pi = 1^-$ solution with β_{31} deformation. On the other hand, for x_{LS} values smaller than 0.7, we obtain $K^\pi = 3^-$ solution with β_{33} deformation. At $x_{LS} = 0.8$, these two configurations mix up in the solution. Therefore, two distinct configurations coexist in the negative parity at the excitation energies of about 10 MeV. In contrast to the ^{20}Ne case, two configurations do not separate but mix up. In such a situation, treatments beyond the present framework seem to be
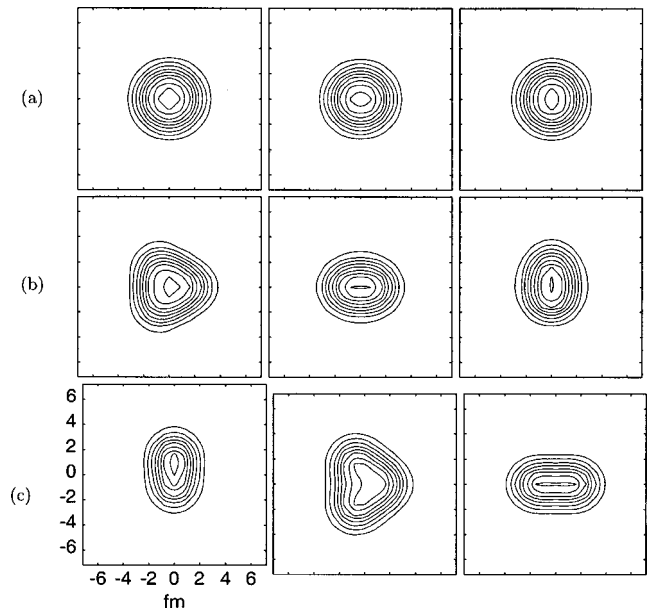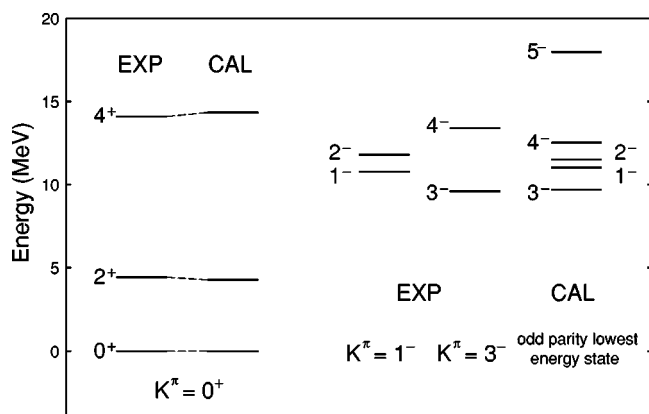

FIG. 4. Density distribution of the internal state in ^{12}C at $x_{LS} = 0.8$ for (a) SHF, (b) PPSHF ($K^\pi = 0^+$), and (c) PPSHF (negative-parity). See the caption of Fig. 1 for explanation.

FIG. 5. Energy spectra of ^{12}C in the AMP.

necessary, for example superposing multiple configurations in the generator coordinate treatment. We leave such an advanced treatment as a future problem.

In summary, we propose the PPSHF method as a useful tool to study both excited and ground states simultaneously.

Self-consistent solutions of the excited states can be obtained in the negative parity, while the positive parity solutions describe the ground state incorporating certain correlation effects beyond the simple mean-field treatment. We show the feasibility of such calculations employing the uniform grid representation in the 3D Cartesian coordinate and achieving the three-dimensional angular momentum projection. The application to two $N=Z$ nuclei, ^{20}Ne and ^{12}C, reveals that the obtained solutions show interesting deformations violating reflection symmetries and incorporating clustering correlation. We will apply, for the future, the present framework for the systematic investigation and predictions of light nuclei, including exotic neutron rich nuclei.

[1] M. Bender, P.-H. Heenen, and P.-G. Reinhard, Rev. Mod. Phys. **75**, 121 (2003).

[2] P. Ring and P. Schuck, *The Nuclear Many Body Problem* (Springer-Verlag, Berlin, 1980), Chap. 11.

[3] S. Takami, K. Yabana, and K. Ikeda, Prog. Theor. Phys. **96**, 407 (1996).

[4] S. Takami, K. Yabana, and K. Ikeda, *Proceedings of the XVII RCNP International Symposium on the Innovative Computational Methods in Nuclear Many-Body Problems* (World Scientific, Singapore, 1998), p. 112.

[5] S. Takami, Ph.D. thesis, Niigata University, 1998.

[6] Y. Fujiwara *et al.*, Prog. Theor. Phys. **68**, 29 (1980).

[7] Y. Kanada-En'yo and H. Horiuchi, Prog. Theor. Phys. Suppl. **142**, 205 (2001).

[8] Y. Kanada-En'yo, Phys. Rev. Lett. **81**, 5291 (1998).

[9] H. Flocard, S. Koonin, and M. Weiss, Phys. Rev. C **17**, 1682 (1978).

[10] T. Duguet and P. Bonche, Phys. Rev. C **67**, 054308 (2003).

[11] Y. M. Engel, D. M. Brink, K. Goeke, S. J. Krieger, and D. Vautherin, Nucl. Phys. **A249**, 215 (1975).

[12] P. Bonche, H. Flocard, P.-H. Heenen, Nucl. Phys. **A467**, 115 (1987).

[13] N. Van Giai and H. Sagawa, Phys. Lett. **106B**, 379 (1981).

[14] S. Takami, K. Yabana, and M. Matsuo, Phys. Lett. B **431**, 242 (1998).

[15] Y. Kanada-En'yo, M. Kimura, and H. Horiuchi, C. R. Phys., **4**, 497 (2003).

[16] M. Bender, H. Flocard, and P.-H. Heenen, Phys. Rev. C **68**, 044321 (2003).

[17] J. Dobaczewski and J. Dudek, Phys. Rev. C **52**, 1827 (1995).

[18] O. Häusser, T. K. Alexander, A. B. McDonald, G. T. Ewans, and A. E. Litherland, Nucl. Phys. **A168**, 17 (1971).

[19] P.-G. Reinhard and H. Flocard, Nucl. Phys. **A584**, 467 (1995).

[20] F. Ajzenberg-Selove, Nucl. Phys. **A248**, 1 (1975).